Diffraction of wavepackets in space and time

2001 J. Phys. A: Math. Gen. 34 6465

(http://iopscience.iop.org/0305-4470/34/33/311)

INSTITUTE OF PHYSICS PUBLISHING JOURNAL OF PHYSICS A: MATHEMATICAL AND GENERAL

J. Phys. A: Math. Gen. **34** (2001) 6465–6480 PII: S0305-4470(01)23549-5

Diffraction of wavepackets in space and time

G Kälbermann

Soil and Water Department, Faculty of Agriculture, Rehovot 76100, Israel

E-mail: hope@vms.huji.ac.il

Received 22 March 2001, in final form 14 June 2001
Published 10 August 2001
Online at stacks.iop.org/JPhysA/34/6465

Abstract

The phenomenon of wavepacket diffraction in space and time is described. It consists in a diffraction pattern whose spatial location progresses with time. The pattern is produced by wavepacket quantum scattering off an attractive or repulsive time-independent potential. An analytical formula for the pattern at $t \to \infty$ is derived both in one dimension and in three dimensions. The condition for the pattern to exist is developed. The phenomenon is shown numerically and analytically for the Dirac equation in one dimension also. An experiment for the verification of the phenomenon is described and simulated numerically.

PACS numbers: 03.65.Nk, 03.65.Pm, 03.75.-b, 03.80.+r

1. Wavepacket diffraction in space and time

The diffraction process is a cornerstone of wave scattering. Quantum mechanical scattering shows diffractive phenomena in space, like nuclear diffractive scattering, and separately in time [1]. The combined effect of time-dependent opening of slits for plane monochromatic waves produces diffraction patterns in space and time [2]. Both diffraction in time and diffraction in space and time are of the utmost importance in testing the validity of time-dependent predictions of quantum mechanics. Recent measurements of atomic wave diffraction [3] have indeed demonstrated that the *diffraction in time* process is supported by experiments.

This paper will show that there exists a broad class of phenomena occurring in nonrelativistic and relativistic quantum wavepacket potential scattering that behave as time-dependent *persistent* diffraction patterns. The patterns are produced by a time-independent potential. In the present case, the pattern will be shown not to decay exponentially, as for the *diffraction in time* phenomenon, and may provide a tool to deepen our understanding of time-dependent quantum processes, pertaining to the description of atomic (or other) beams by means of wavepackets.

The peak structure exists for all packets, but it survives only for packets that are initially narrower than a value related to the potential width. For wider packets, the peak structure merges into a single peak.

The effect is named *wavepacket diffraction in space and time*. It will be shown that the structure exists for repulsive and attractive potentials. It also appears when the relativistically invariant Dirac equation is used instead of the Schrödinger equation.

This paper emerges from numerical investigations of one- and two-dimensional wavepacket scattering off an attractive potential that showed curious multiple-peak structures resembling a diffraction pattern [4, 5]. It was seen there that wavepackets that are narrower than the well width initially backscatter as a wavetrain that is coherent and multiple peaked, a diffraction pattern that travels backwards in one dimension and at large angles in two-dimensions.

The effect is absent for packets whose *initial* width is much larger than the potential extension. For this case, a smooth wave hump proceeds both forwards and backwards. In section 2 we will treat the one-dimensional case analytically. The Dirac scattering in one dimension will be dealt with in section 3. Section 4 generalizes the results of section 2 to three dimensions. In section 5 an experiment aimed at verifying the theoretical predictions will be suggested and simulated. Section 6 summarizes the paper.

2. Wavepacket diffraction in space and time in one dimension

In order to develop an analytical formula for the diffraction pattern, we resort to the simplest possible case that can be dealt with almost completely analytically. This is the example of a wavepacket scattering off a square well.

Consider a Gaussian wavepacket impinging from the left, on a well located around the origin,

$$V(x) = -V_0\,\Theta(w - |x|) \tag{1}$$

where $2w$ is the width, Θ is the Heaviside function and V_0 the depth. The use of a square well facilitates the calculation, but the results do not depend on the sharpness of the well as evidenced by the numerical results of [4]. (Theoretical arguments that support this statement may be found below after equation (7).) Using the results of [6], we can write immediately both the reflected and transmitted packets. From this point on we take $\hbar = c = 1$.

$$\psi(x,t) = \int_{-\infty}^{\infty} \phi(k,x,t)\, a(k,q_0)\, \mathrm{e}^{-\mathrm{i}\frac{k^2}{2m}t}\, \mathrm{d}k \tag{2}$$

where $\phi(k,x,t)$ is the stationary solution to the square-well scattering problem for each k and $a(k,q_0)$ is the Fourier transform amplitude for the initial wavefunction with average momentum q_0.

Explicitly, in the backward direction that interests us here, for $x < -w$

$$\begin{aligned}
&\phi(k,x,t) = D(k,k')\,\mathrm{e}^{\mathrm{i}k(x-x_0)} + F(k,k')\,\mathrm{e}^{-\mathrm{i}k(x+x_0+2w)}\\
&D(k,k') = 1\\
&F(k,k') = \frac{E(k,k')}{A(k,k')}\\
&E(k,k') = -2\,\mathrm{i}\,(k^2 - k'^2)\,\sin(2\,k'w)\\
&A(k,k') = (k+k')^2\,\mathrm{e}^{-2\mathrm{i}k'w} - (k-k')^2\mathrm{e}^{2\mathrm{i}k'w}
\end{aligned} \tag{3}$$

where

$$a(k,q_0) = \mathrm{e}^{-\sigma^2(k-q_0)^2} \tag{4}$$

with $k' = \sqrt{k^2 + 2\,m\,|V_0|}$, and σ the width parameter of the packet.

The integral of the D term can be performed explicitly. We will call this contribution to the wave $\psi_{\rm in}$. For $t \to \infty$ we have

$$\begin{aligned} \psi_{\rm in} &\approx \sqrt{\frac{\pi}{\sigma^2 + {\rm i}\,t/(2\,m)}}\,{\rm e}^{u} \\ u &= {\rm i}\,\frac{m}{2\,t}\,(x - x_0)^2 - \frac{m^2\,\sigma^2}{t^2}\,(x - x_0 - q_0\,t/m)^2. \end{aligned} \tag{5}$$

For long times, the oscillations in the exponent of the term accompanying F in the wavefunction are extremely fast. The most important contributions come from phases that are an extremum with respect to k. We will call the contribution to the wave due to F $\psi_{\rm refl}$. Using the saddle point method we find that, the extremal phase for $\psi_{\rm refl}$ demands the real part of the momenta to be positive for negative x, namely $k_{\rm extremal} \approx \frac{2\sigma^2\,q_0 - {\rm i}\,x}{2\sigma^2 + {\rm i}t/(2\,m)}$.

We concentrate on the case $k' \gg k$, the low-energy regime, for which the polychotomous effect is most visible [4, 5].

At $k \approx 0$ we have $F \approx -1$. To order $\frac{1}{t}$, for long times and distances $x \gg x_0 \gg w$ using the properties of Gaussian integrals it is found that

$$\begin{aligned} \psi_{\rm refl} &\approx \sqrt{\frac{\pi}{\sigma^2 + {\rm i}\,t/(2\,m)}}\,{\rm e}^{\tilde{u}} \\ \tilde{u} &= {\rm i}\,\frac{m}{2\,t}\,(x + x_0)^2 - \frac{m^2\,\sigma^2}{t^2}\,(x + x_0 + q_0\,t/m)^2. \end{aligned} \tag{6}$$

The full wave in the backward direction is obtained from the sum of the interfering waves of equations (5) and (6). The amplitude of the wave for very long times becomes

$$\begin{aligned} |\psi| &= 2\,\sqrt{\frac{2\,m\,\pi}{t}}\,{\rm e}^{-z}\,\left|\sin\left(\frac{m\,x}{t}(x_0 + 2\,{\rm i}\,\sigma^2\,q_0)\right)\right| \\ &= 2\,\sqrt{\frac{2\,m\,\pi}{t}}\,{\rm e}^{-z}\,\sqrt{\sin^2\left(\frac{m\,x\,x_0}{t}\right) + \sinh^2\left(\frac{2\,\sigma^2\,q_0\,m\,x}{t}\right)} \\ z &= \sigma^2\,\left(\frac{m^2\,(x^2 + x_0^2)}{t^2} + q_0^2\right). \end{aligned} \tag{7}$$

This expression represents a diffraction pattern that travels in time and persists. This result hinges upon the value of F as $k \to 0$. However, this value is essentially the reflection amplitude for zero momenta, that is equal to -1 regardless of the potential. Therefore, the expression for ψ above does not depend on the choice of a square well.

Figure 1 shows a comparison of the expression above (without any change in scale) with the numerical calculation of the reflected wave for $t = 1.2 \times 10^7$, a huge time compared to the transit time of the packet through the well. The initial momentum is $q_0 = 0.4$, the well width $w = 1$, the initial position $x_0 = -60$ and the mass parameter $m = 40$. We chose a large mass in order to be on the nonrelativistic domain $\frac{q_0}{m} = v = 0.01$, for which the Schrödinger equation is valid. The figure shows that the theoretical expression and the numerical calculation agree, despite the approximate treatment of the F term. For the longest distances, the approximation is not valid. At these distances the approximation of $k \approx 0$ breaks down. Due to the same time dependence of both the sin and sinh pieces, it is quite clear that the pattern persists to infinite time. The larger x_0, the cleaner the pattern, and more peaks appear in the wavetrain. Clearly for $x_0 \to \infty$, the pattern disappears. The smaller q_0, the more visible—less background—the diffraction pattern is.

In order to understand the absence of diffractive structures for a broad packet we consider the imaginary term inside the sin function in equation (7). We have to estimate the extension

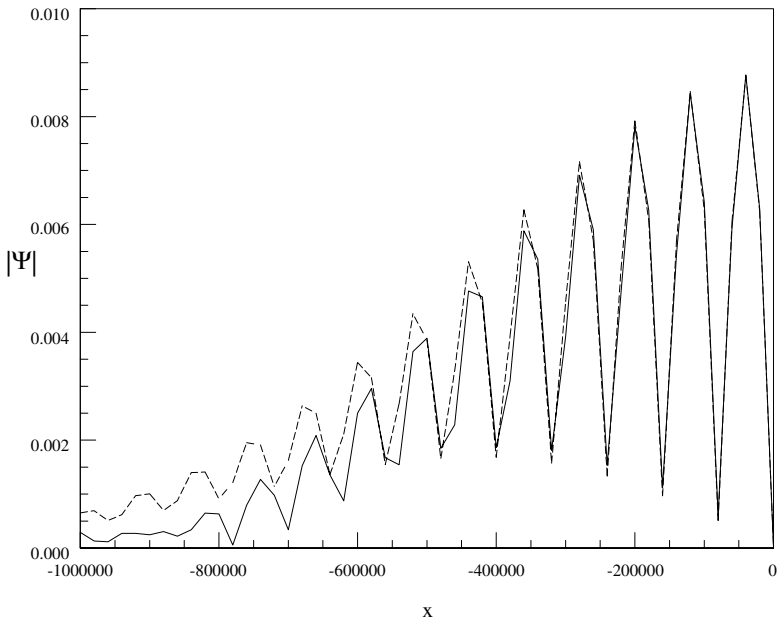

Figure 1. $|\Psi|$ as a function of distance x, numerical calculation (solid curve) and theoretical expression of equation (7) (dashed curve), at $t = 1.2\times10^7$. The wavepacket has average momentum $q = 0.4$, mass $m = 40$, width $\sigma = 0.5$ and initial location $x_0 = -60$. The well parameters are width $w = 1$ and depth $V_0 = 1$.

of the diffraction pattern that changes with time. The momenta involved are $k_{\max} = \frac{m\ |x_{\max}|}{t}$. The constructive interference occurs whenever F of equation (3) does not differ substantially from the value at $k = 0$. At higher momenta F is complex, the real part diminishes and the imaginary part starts increasing. These changes reduce the constructive part of the pattern; incoherent pieces arise that blur the multiple peak behaviour. The faster the drop of the real part of $-F$, the smaller the range of momenta for which the formula above holds.

In figures 2 and 3 we have shown the real and imaginary parts of F for different well depths. Figure 2 corresponds to the case close to a transmission resonance at $k = 0$, $\frac{k'_0\ w}{2\ \pi} = 1.006\,584\,242\,09$ and twice this value, with $k'_0 = \sqrt{2\ m\ |V_0|}$. Figure 3 corresponds to in between two transmission resonances at threshold $\frac{k'_0\ w}{2.25\ \pi} = 0.999\,890\,293\,9413$ and one and a half times this value. Note however that the terminology of transmission resonance refers to a nonzero value of k. There is no transmission at zero momentum. In the actual packet scattering process, even if $k'_0\ w$ is equal to the value of a transmission resonance or in between resonances, k' differs even by a small amount from the threshold value. Therefore our pictures display the expected behaviour of F. Even if for a specific value of k the condition of a transmission resonance is met, this set is of measure zero as compared to the continuum of values of k' entering the calculation of the reflected wave.

We can see from the figures that in either case, close to a transmission resonance or in between resonances, the drop in $-F$ scales as $\frac{1}{w}$. The same is true for any other choice of the product $k'_0 w$. Therefore we can estimate $k_{\max} \approx (2\ w)^{-1}$, with a proportionality factor that depends on the depth of the potential only. As it is our aim to understand the absence of a polychotomous wavetrain for a wide packet and not the exact cut-off, we proceed with the above estimate as a working hypothesis. For the imaginary part of the argument in the

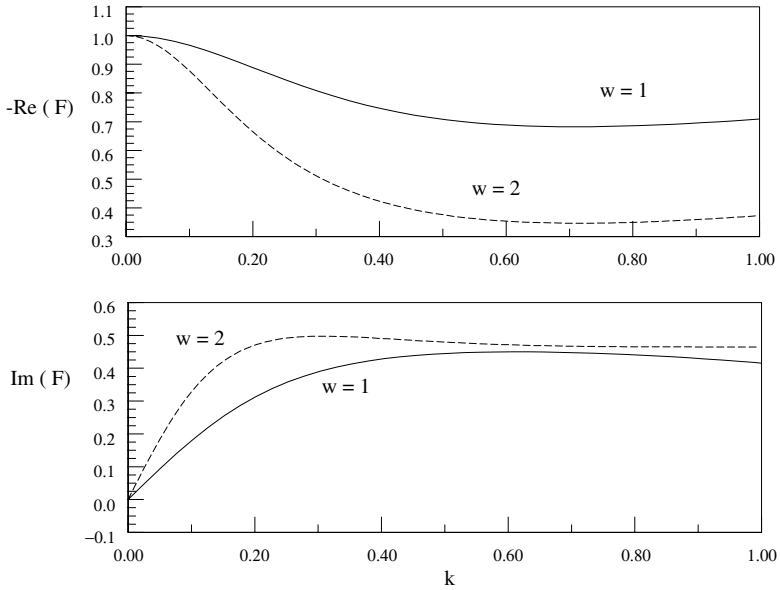

Figure 2. Negative real and imaginary parts of the coefficient F of equation (3) as a function of k for the case $\frac{k_0' w}{2\pi} = 1.006\,584\,242\,09$, $w = 1$, and twice this value, $w = 2$.

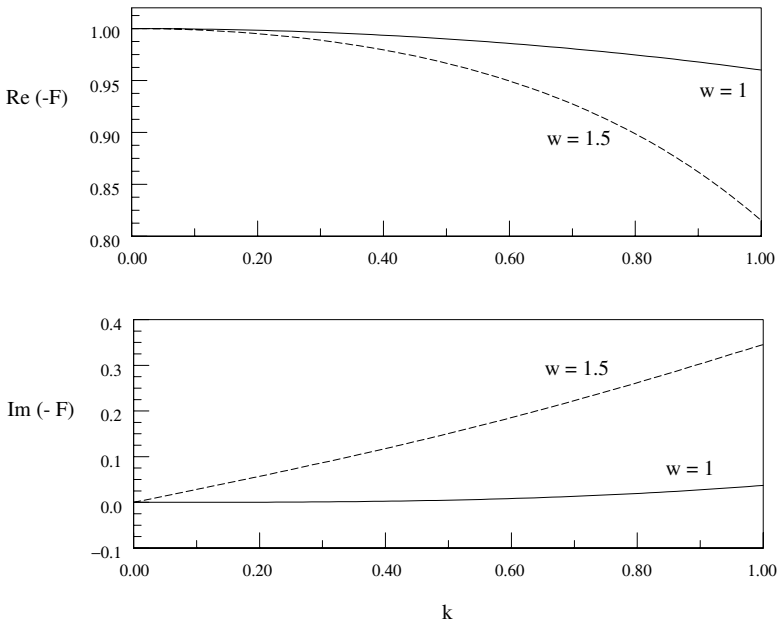

Figure 3. Real and imaginary parts of the coefficient $-F$ of equation (3) as a function of k for the case $\frac{k_0' w}{2.25\,\pi} = 0.999\,890\,293\,9413$, $w = 1$, and 1.5 times this value, $w = 1.5$.

sin function in equation (7) to stay small and not blur up completely the pattern we need $2\,k_{\max}\,\sigma^2\,q_0 \ll 1$, or, using our scaling argument,

$$\sigma \ll \sqrt{\frac{w}{q_0}}. \tag{8}$$

For a fixed incoming momentum, the initial packet width has to be smaller than a certain proportion of the well width. This was indeed observed in numerical simulations [4]. The interference between incoming and reflected waves, D and F terms in equation (3), is responsible for the diffractive pattern. The transmitted wave has no such two components. There is no possible interference and no diffraction peaks may be observed in the transmitted packet.

All the above arguments pertain only to the specific example presently considered. However, the example carries the essential ingredients for any type of packet. One only needs to replace the form factor e^{-z} in equation (7) by the corresponding expression for any other chosen packet. It does not depend on the type of potential. Other functional dependences may give more complicated expressions than the simple sin function above, but essentially they will show the same structure.

The all-important contribution to the diffraction in space and time arises from the interference between the incoming packet and the reflected wave originating from momenta $k \to 0$. The latter amounts to the excitation of a virtual state at almost zero energy quasi-bound state inside the well, as was indeed observed numerically in [4, 5]. The extreme importance of zero-energy metastable states inside the well has been recognized in the literature for quite some time. In the limit of $k = 0$, the virtual state becomes a half-bound state. This state is usually termed a half-bound state due to a factor of one-half in the phase shift at threshold in the derivation of Levinson's theorem in the nonrelativistic case [7], and the relativistic case of the Dirac equation [8]. Its existence affects the phase shift at threshold. This paper shows that the existence of metastable almost zero-energy virtual states makes itself evident through wavepacket diffraction in space and time. The effect should be independent of the sign of the potential. Transforming to a barrier is like transforming a slit to an obstacle (Babinet's principle). Both show diffraction in space. Therefore, we should see diffraction in space and time for barriers too, provided the width of the barrier is smaller than the initial width of the packet. This is indeed the case as shown in figures 4 and 5.

A minimal uncertainty Gaussian wavepacket travelling from the left with an average speed v, initial location x_0, mass m, wave number $q = m\,v$ and width σ,

$$\psi = C\,\exp\left(\mathrm{i}\,q\,(x - x_0) - \frac{(x - x_0)^2}{4\,\sigma^2}\right) \tag{9}$$

is scattered from a Gaussian barrier

$$V(x) = V_0\,\exp\left(-\frac{x^2}{w^2}\right). \tag{10}$$

Let us now compare this with the phenomenon of *diffraction in time* [1], and *diffraction in space and time* with plane waves [2, 9]. The former arises when a shutter is suddenly opened at $t = 0$. Behind the shutter there is a stream of monoenergetic particles. After the opening of the shutter, there arise oscillations in the current on the other side of it. These oscillations die out at large times. The latter is produced by the combined effect of shutters that open in time and interfere between them in space, or other variations [2]. Instead of having a vanishingly small time correlation length [10], the process of wavepacket diffraction in space and time persists for infinite time. However, for the polychotomous pattern to survive we need an initial spread of the packet smaller than the extent of the potential. Translating to a framework of timescales, this would imply that the timescale of the opening of the shutter should be longer than the timescale generated from the width of the packet, namely $\Delta t_{\mathrm{shutter}} > \frac{\sigma\,m}{q_0}$, where, as

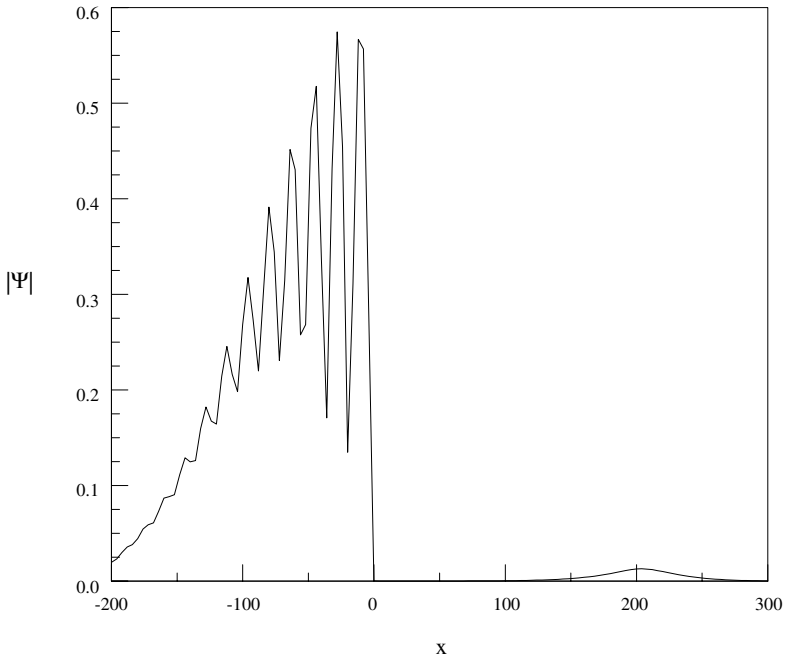

Figure 4. $|\Psi|$ as a function of distance x for an initial wavepacket of width $\sigma = 0.5$ starting at $x_0 = -10$ impinging upon a barrier of width parameter $w = 1$ and height $V_0 = 0.2$ at $t = 800$; the initial average momentum of the packet is $q = 1$.

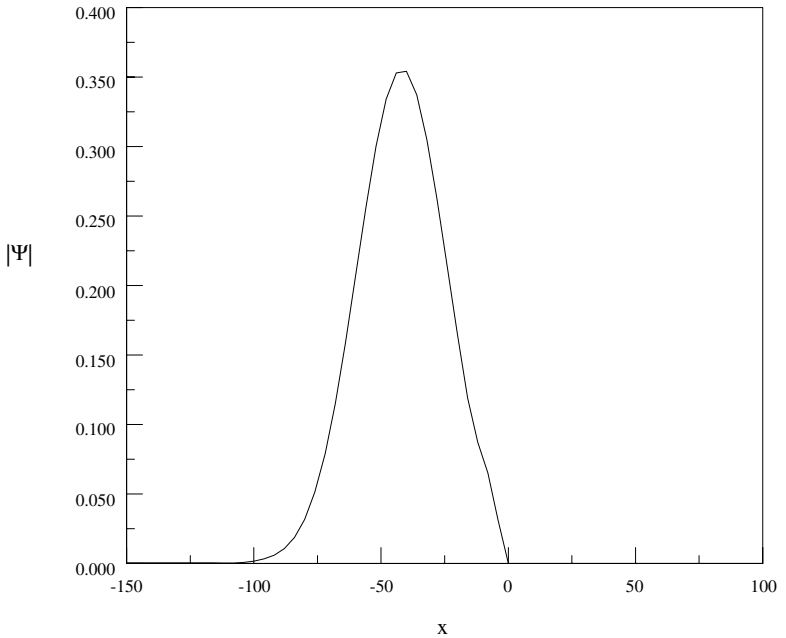

Figure 5. $|\Psi|$ as a function of distance x for an initial wavepacket of width $\sigma = 2$ starting at $x_0 = -10$ impinging upon a barrier of width parameter $w = 1$ and height $V_0 = 0.2$ at $t = 1200$; the initial average momentum of the packet is $q = 1$.

above, σ is the initial width of the packet. It appears interesting to find out whether a finite opening time may prevent the exponential decay of the diffraction in time process also.

3. Diffraction in space and time for the Dirac equation

The diffraction in time phenomenon [1] does not exist in the relativistic case. This can be seen from equations (18) and (34) in [1] for the ordinary wave equation and the Klein–Gordon (KG) equation respectively. Only when the speed of light is taken to infinity are the nonrelativistic results recovered, as can be seen from equation (36) in the same work. This seems quite surprising, because the KG equation at low momenta compared to the mass yields very similar phenomena as the corresponding Schrödinger equation, as evidenced by a substitution $\psi_{\mathrm{KG}} = \mathrm{e}^{-\mathrm{i}mt}\psi_{\mathrm{Schrödinger}}$. It is not possible to open a shutter in zero time, as this implies an infinite opening speed. A shutter that opens slowly enough may provide a framework not only in which the pattern persists to long times, but which allows its existence for the relativistic case in a causal manner too.

In order to see that wavepacket diffraction in space and time does exist in the relativistic case, we performed numerical calculations using the one-dimensional Dirac equation with a scalar potential[1] $S(x)$ as given in equation (10)

$$\left[\mathrm{i}\gamma^{\mu}\,\partial_{\mu} + (m + S(x))\right]\Psi = 0. \tag{11}$$

For the initial packet we took a minimal uncertainty relativistically invariant wavepacket

$$\begin{aligned} \Psi_0 &= \begin{pmatrix} U \\ V \end{pmatrix} \\ U &= \int \mathrm{d}k\, \mathrm{e}^{\mathrm{i}k(x-x_0)-2\sigma^2(EE_0-kq_0-m^2)} \\ V &= \int \mathrm{d}k\, \frac{\mathrm{i}k}{E+m} \mathrm{e}^{\mathrm{i}k(x-x_0)-2\sigma^2(EE_0-kq_0-m^2)} \end{aligned} \tag{12}$$

with $E = \sqrt{k^2+m^2}$, $E_0 = \sqrt{q_0^2+m^2}$, and we have taken $\gamma_{\mathbf{0}} = \sigma_z$, $\gamma_{\mathbf{1}} = \sigma_z\sigma_x$ for the Dirac matrices, where σ denotes the corresponding Pauli matrix.

We extended the numerical method used for the nonrelativistic case [11] to the unitary evolution of the Dirac particle and found it extremely accurate. This method is a straightforward extension of the method of [11][2]. The vector density $\rho = \int \mathrm{d}x\, (|U|^2 + |V|^2)$ is conserved to an accuracy of more than 0.1% after millions of iterations. The equation is solved with high accuracy as determined not only by substitution, but also by comparing with the free evolution of the wavepacket above at large times. The price one has to pay for the Dirac case is a much smaller time increment because of the oscillations introduced by the mass parameter. Figures 6 and 7 show the results obtained.

It is clear from the figures that the phenomenon exists in the Dirac case also.

We now proceed to study the analytical behaviour of the diffraction process for the Dirac equation. Consider the one-dimensional Dirac equation with a scalar potential only $S(x)$ as given by equation (11). For the initial packet we use a minimal-uncertainty relativistically invariant wavepacket of equation (12). The stationary wavefunction inside and outside the

[1] The use of a potential in the non-stationary case for relativistic equations is questionable. However, it is still of relevance.

[2] A numerical algorithm and routines are available from the author.

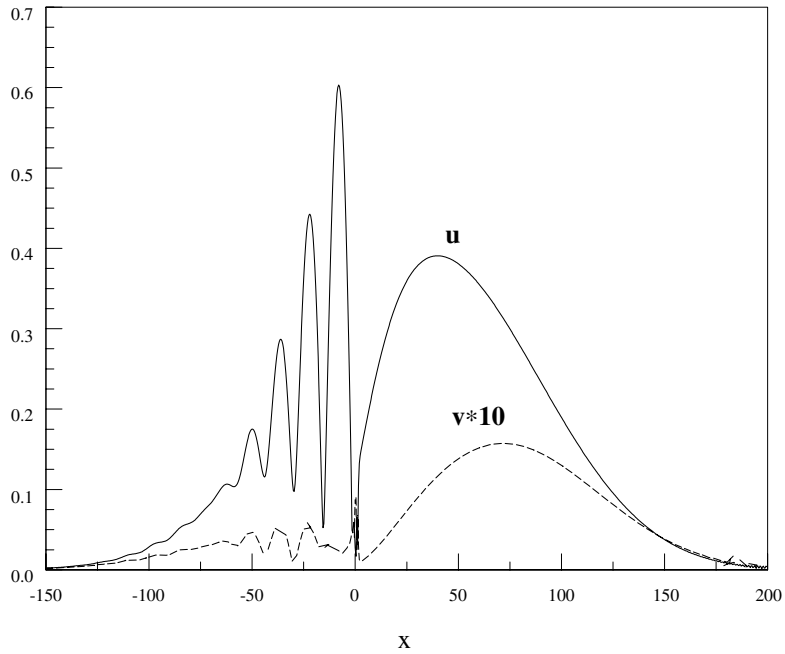

Figure 6. Upper $u = |U|$ and ten times lower component $v = |V|$ of the Dirac wavefunction for an initial wavepacket of width $\sigma = 0.5$ starting at $x_0 = -10$, $q_0 = 1$ on a well of width parameter $w = 1$ and depth $V_0 = 1$ at $t = 800$.

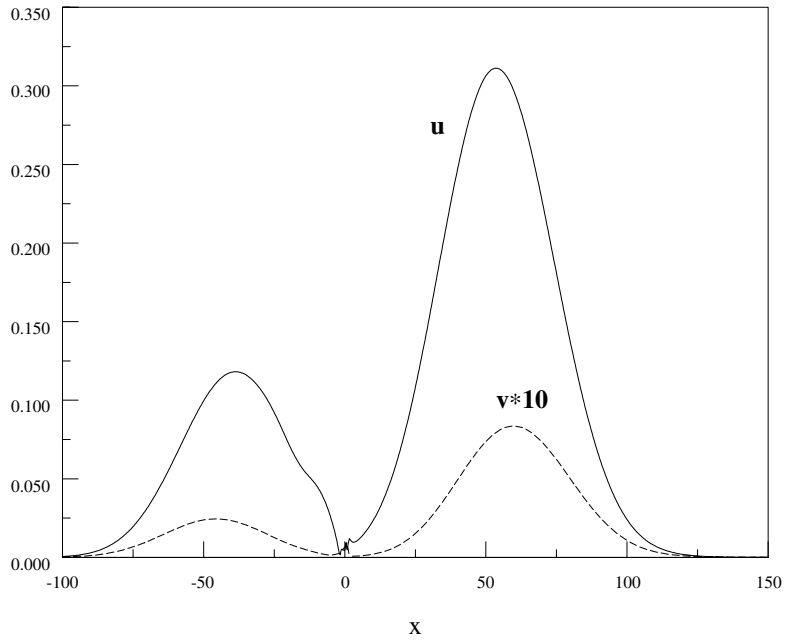

Figure 7. Upper $u = |U|$ and ten times lower component $v = |V|$ of the Dirac wavefunction for an initial wavepacket of width $\sigma = 2$ starting at $x_0 = -10$, $q_0 = 1$ on a well of width parameter $w = 1$ and depth $V_0 = 1$ at $t = 1200$.

well for fixed momentum is given by $\phi(k,x,t) = \begin{pmatrix} \phi_1\, \mathrm{e}^{-\mathrm{i}Et} \\ \phi_2\, \mathrm{e}^{-\mathrm{i}Et} \end{pmatrix}$

$$\begin{aligned}
&\phi_1(x < -w, k, t) = (\mathrm{e}^{\mathrm{i}kx} + B\mathrm{e}^{-\mathrm{i}kx}) \\
&\phi_2(x < -w, k, t) = \frac{\mathrm{i}\,k}{E+m}\,(\mathrm{e}^{\mathrm{i}kx} - B\mathrm{e}^{-\mathrm{i}kx}) \\
&\phi_1(-w < x < w, k, t) = (C\mathrm{e}^{\mathrm{i}k'x} + D\mathrm{e}^{-\mathrm{i}k'x}) \\
&\phi_2(-w < x < w, k, t) = \frac{\mathrm{i}\,k'}{E+m^*}\,(C\mathrm{e}^{\mathrm{i}k'x} - D\mathrm{e}^{-\mathrm{i}k'x}) \\
&\phi_1(w < x, k, t) = F\,\mathrm{e}^{\mathrm{i}kx} \\
&\phi_2(w < x, k, t) = \frac{\mathrm{i}\,k}{E+m}\,F\,\mathrm{e}^{\mathrm{i}kx}
\end{aligned} \tag{13}$$

with

$$\begin{aligned}
B &= \frac{(1-g^2)(e_3^2 - e_4^2)}{\Delta} \\
C &= \frac{-2\,e_1\,e_4\,(1+g)}{\Delta} \\
D &= \frac{2\,e_1\,e_3\,(1-g)}{\Delta} \\
F &= \frac{-4\,g}{\Delta}
\end{aligned} \tag{14}$$

where[3] $e_1 = \mathrm{e}^{\mathrm{i}kw}$, $e_2 = \mathrm{e}^{-\mathrm{i}kw}$, $e_3 = \mathrm{e}^{\mathrm{i}k'w}$, $e_4 = \mathrm{e}^{-\mathrm{i}k'w}$, $g = \frac{k'\,(E+m)}{k\,(E+m^*)}$, $\Delta = e_3^2\,(1-g)^2 - e_4^2\,(1+g)^2$ and $k' = \sqrt{E^2 - (m^*)^2}$, $m^* = m - V_0$.

The solution to the scattering of the packet becomes $\Psi(x,t) = \begin{pmatrix} U(x,t) \\ V(x,t) \end{pmatrix}$

$$\begin{aligned}
U(x,t) &= \int \mathrm{d}k\,\phi_1(k,x,t)\,\mathrm{e}^{-\mathrm{i}kx_0 - 2\sigma^2(EE_0 - kq_0 - m^2) - \mathrm{i}Et} \\
V(x,t) &= \int \mathrm{d}k\,\phi_2(k,x,t)\,\mathrm{e}^{-\mathrm{i}kx_0 - 2\sigma^2(EE_0 - kq_0 - m^2) - \mathrm{i}Et}.
\end{aligned} \tag{15}$$

As in section 2 we consider the long-time behaviour of the wave. Here too, the reflected wave will receive contributions mainly from low values of k. On inspection of the reflection parameter B in equation (14), we find that for $k \to 0$, $B \to -1$. The same happened in the nonrelativistic treatment of section 2. For low initial momenta, $q_0 \ll m$, or $v \ll 1$, the exponential of equation (15) becomes $\approx \mathrm{e}^{-\mathrm{i}k\,x_0 - \mathrm{i}mt - \mathrm{i}\frac{k^2}{2m}t - \sigma^2(q_0-k)^2}$. So except for the factor $\mathrm{e}^{\mathrm{i}\,m\,t}$, that is independent of k, we are back at the nonrelativistic case for the upper component, and at the same time the lower component vanishes. Hence, the Dirac case in one dimension is exactly analogous to the nonrelativistic case for low average momenta of the initial wavepacket.

In the ultrarelativistic limit $m \to 0$, the upper and lower components are identical up to a factor of i. The incoming and reflected waves do not spread. Hence, there is no interference between the two. If we first find the wave in the backward direction as in section 2, and then take the limit of a small mass, we find that the pattern disappears, as the arguments of the sin function tend to zero. For $t \to \infty$, the backwards scattered wave becomes a receding wavepacket located around $x = -x_0 - t - w$, without any diffraction. The incoming packet is no longer present in the region behind the well.

[3] For a vector potential the * is in the energy instead of the mass.

In summary, the diffraction in space and time with wavepackets exists in the relativistic regime, but gradually diminishes as the mass decreases, until it is eventually washed out completely for the massless case, as was found for the *diffraction in time* process with the KG equation [1].

4. Wavepacket diffraction in three dimensions

In section 2 it was shown analytically that there exists a broad class of phenomena occurring in nonrelativistic and relativistic quantum wavepacket potential scattering that behave as time-dependent *persistent* diffraction patterns. The patterns are produced by a time-independent well or barrier. Differing from the *diffraction in time* [1] and *diffraction in space and time* [2] phenomena, that apply to the time-dependent opening of slits with plane monochromatic waves, the pattern does not decay exponentially with time.

We now consider the generalization of the analytical formula of equation (7) to three dimensions. We take a Gaussian wavepacket in three dimensions,

$$\begin{aligned} &\phi(\vec{r}, t) = \mathrm{e}^{y_0} \\ &y_0 = \mathrm{i}\,\vec{q}_0 \cdot\ (\vec{r} - \vec{r}_0) - \frac{(\vec{r} - \vec{r}_0)^2}{4\,\sigma^2} \end{aligned} \tag{16}$$

with $\vec{q}_0$, the initial average momentum of the packet, $\vec{r}_0$, the initial location and σ the packet width, impinging on a spherically symmetric square well

$$V(x) = -V_0\ \Theta(w - r) \tag{17}$$

where w is the well width, V_0 the depth and Θ the step function. The results are not dependent on the choice of wavepacket however; the Gaussian profile facilitates the integrations. The total wavefunction with outgoing boundary condition at large distances reads [12]

$$\begin{aligned} \psi^+(\vec{r}, t) &= \psi_{\mathrm{in}}(\vec{r}, t) + \psi_{\mathrm{scatt}}(\vec{r}, t) \\ &= \int \mathrm{d}^3k\ f(\vec{k}, \vec{q}_0)\ (\psi_{\mathrm{in}}(\vec{k}, \vec{r}, t) + \psi_{\mathrm{scatt}}(\vec{k}, \vec{r}, t)) \end{aligned} \tag{18}$$

where

$$\begin{aligned} &\psi_{\mathrm{in}}(\vec{k}, \vec{r}, t) = \mathrm{e}^{\mathrm{i}\vec{k}\cdot\vec{r}} \\ &\psi_{\mathrm{scatt}}(\vec{k}, \vec{r}, t) = \frac{\mathrm{e}^{\mathrm{i}kr}}{kr} \sum_L (2L + 1)\ \mathrm{e}^{\mathrm{i}\delta_L}\ \sin(\delta_L)\ P_L(\hat{r} \cdot \hat{k}) \\ &f(\vec{k}, \vec{q}_0) = \mathrm{e}^{-(\vec{k} - \vec{q}_0)^2\sigma^2 - \mathrm{i}\vec{k}\cdot\vec{r}_0 - \mathrm{i}\frac{k^2}{2m}t}. \end{aligned} \tag{19}$$

The incoming wave may be found explicitly to be

$$\begin{aligned} &\psi_{\mathrm{in}} = \left(\frac{\pi}{\mathrm{i}t/(2m) + \sigma^2}\right)^{3/2}\ \mathrm{e}^{y_1}\ \mathrm{erfc}\left(-\mathrm{i}\frac{D}{\sqrt{\sigma^2 + \mathrm{i}t/(2m)}}\right) \\ &y_1 = -\frac{D^2}{4\ (\mathrm{i}\,t/(2m) + \sigma^2)} - q_0^2\,\sigma^2 \end{aligned} \tag{20}$$

where $D = |\vec{r} - \vec{r}_0 - 2\,\mathrm{i}\,\sigma^2\vec{q}_0|$, erfc represents the complementary error function of the complex argument and the absolute value in the definition of D pertains to the vectorial character, and not to the complex number. Error functions and similar Fresnel integrals are found in many diffraction formulae, such as those appearing in the works of Moshinsky [1].

Performing the angular integral over $\hat{\boldsymbol{k}}$, the scattered wave becomes

$$\begin{aligned}\psi_{\rm scatt}(\vec{r},t) &= \int k^2\,{\rm d}k\;\Phi(\vec{r},k,t)\\ \Phi(\vec{r},k,t) &= \sqrt{4\pi}\;\frac{{\rm e}^{{\rm i}kr}}{k\;r}{\rm e}^{-\sigma^2(k^2+q_0^2)-{\rm i}t\frac{k^2}{2m}}\sum_{L,M}(2L+1){\rm e}^{{\rm i}\delta_L}\,\sin(\delta_L)I_{L,M}(k,\vec{q}_0,\vec{r}_0,\vec{r})\end{aligned} \tag{21}$$

where

$$I_{L,M}(k,\vec{q}_0,\vec{r}_0,\vec{r}) = (4\pi)^2\sum_{l,l',m,m'}{\rm i}^{l'-l}\;C_{l,L}\;j_l(k\;x_0)\;j_{l'}(-2{\rm i}\sigma^2 q_0 k)\;Y_L^M(\hat{r})\;Y_l^{m*}(\hat{r}_0)\;Y_{l'}^{m'*}(\hat{q}_0)$$

$$C_{l,L} = \frac{\sqrt{(2\,l+1)\;(2\,l'+1)}}{\sqrt{(2\;L+1)}}\langle l\;l'\;L|0\;0\;0\rangle\langle l\;l'\;L|m\;m'\;M\rangle. \tag{22}$$

Here Y_l^m represents as usual the spherical harmonics, j_l denotes the spherical Bessel function for complex argument, and $\langle l\;l'\;L|\ldots\rangle$ represents the Clebsh–Gordan coefficient.

The expression for I_L is quite involved. However, for $L=0$ it simplifies considerably. Fortunately, this is the only contribution we need at long times, except for very specific cases for which the phase shift of higher partial waves dominates. For $t\to\infty$ the integral in equation (21) oscillates wildly, except for values of k that give an extremal phase [6]. It is easy to show that in this case only extremely small values of k enter the integral. However, for very small values of k, it reads [12]

$$\begin{aligned}\tan(\delta_l) &= -\frac{(k\;w)^{2\;l+1}}{(2\;l-1)!!\;(2\;l+1)!!}\;\frac{z_l-l}{z_l+l+1}\\ z_l &= \frac{x\;j_l'(x)}{j_l(x)}\end{aligned} \tag{23}$$

where $x = k'\;w = \sqrt{k^2+2\;m\;|V_0|}\;w$, and j_l denotes the spherical Bessel function of order l. Except for very specific cases for which there is a resonance at a higher partial wave, only the lowest partial wave matters. Higher partial waves are suppressed by factors of the form $\left(\frac{w}{\sqrt{{\rm i}t/(2m)+\sigma^2}}\right)^l$. For very long times we can then approximate the scattered wave by taking only the $L=0$ term in equation (21). For this case I_L becomes

$$\begin{aligned}I_0 &= 4\pi\;j_0(kd)\\ d &= |\vec{r}_0+2\;{\rm i}\;\sigma^2\vec{q}_0|\end{aligned} \tag{24}$$

where again the absolute value pertains to the vectorial character of the variable inside the vertical bars, and not to the complex number. Therefore, j_0 is really a complicated mixture of Bessel and Hankel functions.

Inserting equations (24) and (23) in (21) and recalling the rules for the integration of the error function for complex variables, we find the transparent result

$$\begin{aligned}\psi_{\rm scatt} &= -\frac{u_0}{d}\left(\frac{\pi}{{\rm i}t/(2m)+\sigma^2}\right)^{\frac{3}{2}}{\rm e}^{-q_0^2\sigma^2}\left(\frac{r+d}{2\;r}\;{\rm e}^{\lambda_1^2}\;{\rm erfc}(-\lambda_1)-\frac{r-d}{2\;r}\;{\rm e}^{\lambda_2^2}\;{\rm erfc}(-\lambda_2)\right)\\ \lambda_1 &= {\rm i}\frac{(r+d)}{2\sqrt{({\rm i}t/(2m)+\sigma^2)}}\\ \lambda_2 &= {\rm i}\frac{(r-d)}{2\sqrt{({\rm i}t/(2m)+\sigma^2)}}\end{aligned} \tag{25}$$

with $u_0 = w\left(1-\frac{\tan(\kappa\;w)}{\kappa\;w}\right)$, $\kappa=\sqrt{2\;m\;|V_0|}$ and d as defined in equation (24).

The incoming and scattered waves interfere in the total wave. Noting that the scattered wave depends on the absolute value of $\vec{r}$, while the incoming wave depends on $\vec{r}$ itself, it is clear that there will be a different behaviour at forward and backward angles.

For long times and long distances we can safely approximate the complementary error functions with the value erfc ≈ 2. In order to relate to the results of the one-dimensional case, we will bring in here the expression for the full wave, in the case of a packet impinging from a distance r_0 at zero impact parameter, initial momentum q_0, on a well located at the origin. Using equations (20) and (25) we find

$$\begin{aligned}\psi &= 2\,\mathrm{i}\left(\frac{\pi}{\mathrm{i}t/(2m)+\sigma^2}\right)^{3/2} \mathrm{e}^{\alpha}\sin\left(\frac{m\,r}{t}\,(r_0+2\,\mathrm{i}\,q_0\sigma^2)+\mathrm{i}\alpha\right)\,\mathrm{e}^{x}\\ \mathrm{e}^{\alpha} &= \sqrt{\frac{u_0\,(2\,d+\,u_0)}{d^2}}\\ x &= -q_0^2\sigma^2-\frac{r^2\,m^2}{t^2}\sigma^2+\mathrm{i}\frac{m}{2\,t}\,r^2.\end{aligned} \tag{26}$$

This is a diffraction pattern that travels in time as found for the one-dimensional case. Again the pattern becomes blurred and forms a single peak when the imaginary part of the argument of the sin function is large. As explained in section 2, this amounts to the condition $\sigma \gg \sqrt{\frac{w}{q_0}}$. There is here the additional blurring effect of the phase α. For narrow enough packets the pattern persists to infinity.

The results are independent of the impact parameter provided the initial packet is located at a much longer distance along the direction of $\vec{q}_0$ as compared with the transverse direction, as found numerically in [5]. Also the pattern does not depend strongly on the initial energy, as long as it stays small compared with the well depth or barrier height. The formula of equation (26) may be used to find the angular distribution, the scattering and total cross sections etc. Such expressions do not seem to exist in the literature for packets, even for the simplest square-well case dealt with here.

The present treatment took advantage of the properties of Gaussian packets and the simplicity of the square well. However, they are general. One has only to replace the Gaussian form factor by the appropriate one for the case and the phase shift for the square well by the one corresponding to the specific choice of potential. The case of long-range potentials however deserves some care.

In order to visualize somehow the three-dimensional results we present in figure 8 a hypothetical scattering event of a cold neutron packet of 1 Fermi width, with initial velocity of $v = 0.02c$ impinging along the x-axis on a well located around the origin of width 10 Fermi and depth 40 MeV. The initial position of the neutrons is taken to be $x_0 = -20$ Fermi, y_0 (the impact parameter) $= 2$ Fermi and the time is taken to be $t = 5 \times 10^{14}$ also in Fermi units. The numbers are taken just for the sake of exemplification and are unrealistic experimentally regarding the initial width of the packet. For a more viable experimental setup see section 5. We chose the potential range and width to give a large scattered wave contribution. Figure 8 depicts the wave amplitude obtained by adding equations (20) and (25) as a function of distance in metres and we have multiplied the wavefunction by a factor of $(\mathrm{i}t/(2m)+\sigma^2)^{3/2}$, in order to have ordinates with values around $|\psi| = 1$. We have chosen to show graphs for the plane $z = 0$. The pictures are similar for other planes. The darkened elements in the figure are due to fast oscillations of the wave. For this very advantageous choice of parameters the diffraction in space and time in three dimensions exists at all angles and not only in the backward direction. Perhaps this is expected for a very low-speed packet that essentially spreads around a position close to the origin, while a secondary scattered wave interferes with it. Directionality is here weak, in contradistinction to the one-dimensional case. The effect depends strongly on the input parametes. In figure 9 we modified the parameters of figure 8 only slightly by increasing the well depth by 5%. The effects are

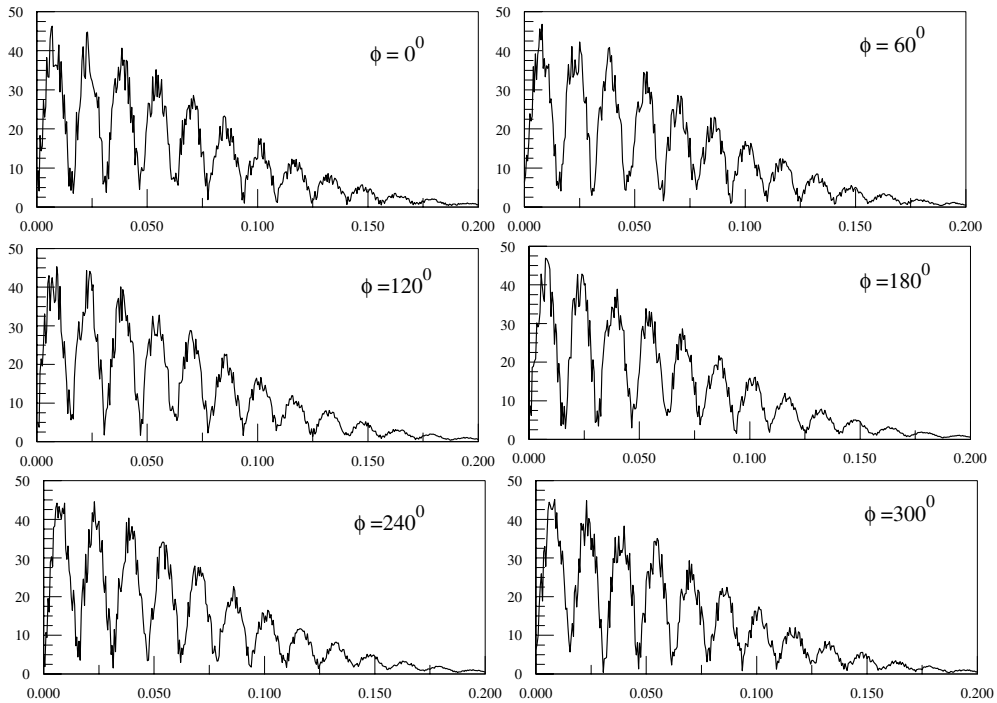

Figure 8. $|\psi|$ as a function of distance for various polar angles ϕ and in the plane $z = 0$ for three-dimensional scattering (see text).

dramatic. Wild oscillations in small regions of space arise. This topic will be studied in a later work.

5. Numerical simulation of a suggested experiment

Present advances in Bose traps permit the handling of atoms at very low temperature and velocities. At such energies the atoms move as if they were a wavepacket provided the random agitation due to thermal effects is not as crucial. However, still the large number of interactions between the particles and between them and the environment causes a decoherence of the wave in quite a short time. Instead of resorting to a cold Bose gas, we will then focus on a drop of liquid helium. Although the experimental details are beyond the expertise of the author, a hypothetical setup will be described in the hope that it is not too far away from reality.

We will imagine a setup that may be dealt with approximately as a one-dimensional system, namely a drop of liquid helium put on a surface a short distance apart from an impervious wall and far from any other boundary, inside a adiabatic container. Gravity is supposed to hold the drop in place vertically. The wall serves as a potential barrier and we are only interested in the horizontal spread of the drop due to the interaction with the wall.

Consider a drop of liquid helium, of around 1 cm^3 in volume lying near a corner of caesium coated plates perpendicular to each other, which may be appropriate for this purpose. Caesium is needed in order to prevent wetting [13]. The helium, plate and environment should be at a temperature below the λ point, although it would be interesting to see the effect of the normal to superfluid component of the helium on the wavepacket behaviour, as a tool to

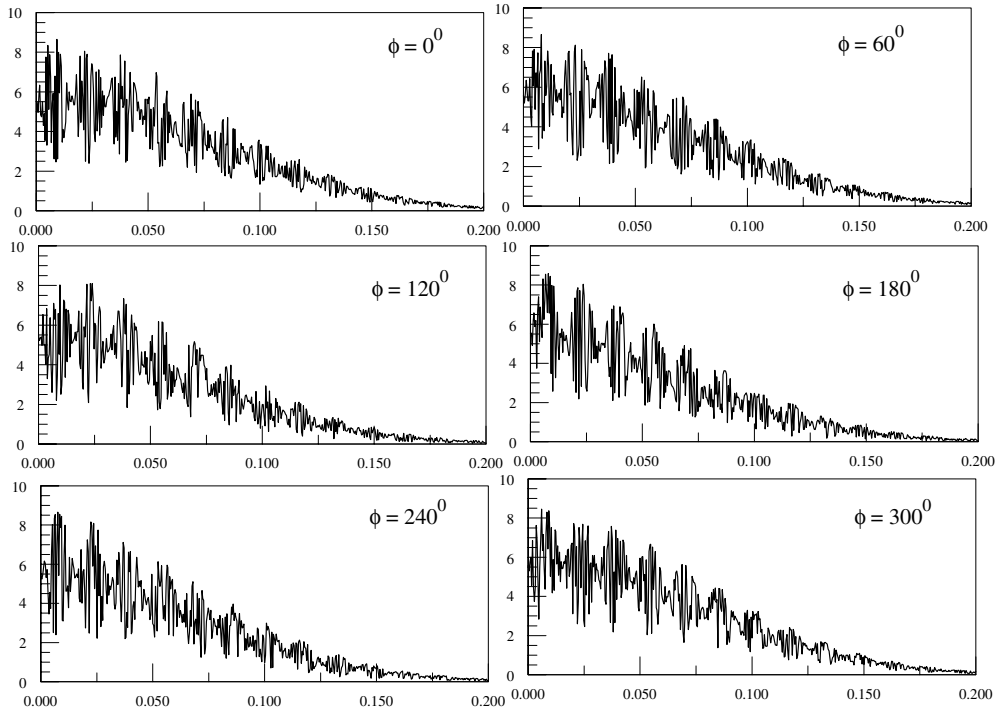

Figure 9. $|\psi|$ as a function of distance for various polar angles ϕ and in the plane $z = 0$ for three-dimensional scattering. Well depth increased by 5% as compared to the previous figure.

study decoherence. Put a large-area detector far behind the drop and the plate. The number of particles measured as a function of time at a fixed position would then be determined by the absolute value of the wavefunction at that point. The particles are repelled by the wall and the packet spreads at the same time.

Figure 10 depicts such a case. We solved the one-dimensional Schrödinger equation for a packet as described in section 2, with a barrier of very large strength. We assumed a total number of particles of $N = 5 \times 10^{21}$, obtained from the tabulated density of liquid helium and a volume of 1 cm^3. We used a plate (potential) of width $w = 1$ cm and strength $V_0 = 4$ eV $\approx 10^{15}$, in units of $\hbar = 1$. We took a detector size of $\mathrm{d}x = 1$ mm, and recorded the amplitude of the wave multiplied by $\mathrm{d}x$ in order to calculate the relative number of particles in the same distance and at varying time. The number of particles as a function of time-relative number multiplied by the total initial number in the drop for a properly normalized wave initially is shown in the figure.

It appears that, due to the large number of particles to be detected, a simple weighing technique might be feasible; in this way we also avoid interaction of the packet with the detector.

It is perhaps too optimistic to expect that the proposed experiment will work as cleanly as in the simulation, due to all kinds of effect inside the drop that lead to decoherence, for example production of internal excitations such as rotons and vortices. However, some remainder of the effect might still show up in the counter. If it does, it will be a triumph for the quantum mechanical description of matter waves by means of wavepackets of macroscopic size.

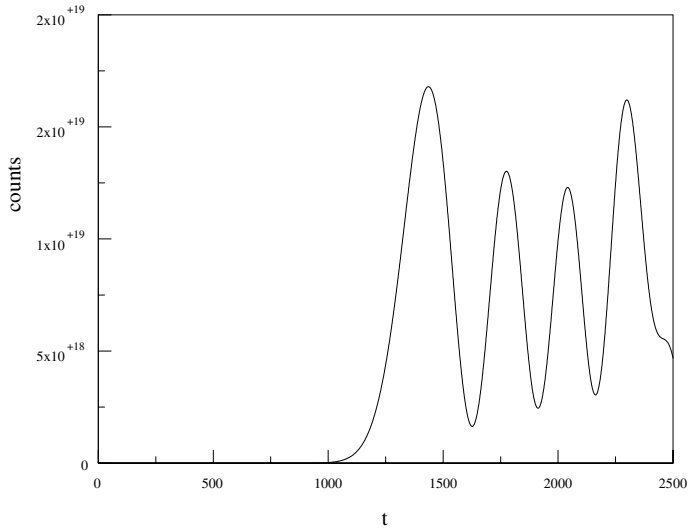

Figure 10. Number of helium atoms counted at a distance of 5 cm behind a plate of thickness $w = 1$ cm as a function of time in seconds.

6. Summary

In summary, we have found in this paper that the phenomenon of diffraction of wavepackets in space and time is determined by the spreading of the incoming waves and the subsequent interference between incoming and scattered waves as well as by the physical size of scatterers. It appears, then, that the theoretical and experimental study of wavepacket scattering as it evolves in time gives us a new tool for the investigation of structure and dynamics of atoms and nuclei and a new possible testground for the predictions of quantum mechanics.

Acknowledgment

The anonymous referee's very constructive remarks are greatly appreciated.

References

[1] Moshinsky M 1952 *Phys. Rev.* **88** 625
For more recent works, see for example:
Xiao M 1999 *Phys. Rev.* E **60** 6226
[2] Brukner C and Zeilinger A 1997 *Phys. Rev.* A **56** 3804 and references therein
[3] Szriftgiser P, Guéry-Odelin D, Arndt M and Dalibard J 1997 *Phys. Rev. Lett.* **77** 4
[4] Kälbermann G 1999 *Phys. Rev.* A **60** 2573
[5] Kälbermann G 2001 *J. Phys. A: Math. Gen.* **34** 3841
(Kälbermann G 1999 *Preprint* quant-ph 9912042)
[6] Bohm D 1951 *Quantum Theory* (New York: Prentice-Hall) p 259
[7] de Bianchi M S 1994 *J. Math. Phys.* **35** 2719
[8] Dong S, Hou X and Ma Z 1998 *Phys. Rev.* A **58** 2160
[9] Felber J, Müller G, Gähler R and Golub R 1990 *Physica* B **162** 191
[10] Gähler R, Felber J, Mezei F and Golub R 1998 *Phys. Rev.* A **58** 280
[11] Goldberg A, Schey H M and Schwartz J L 1967 *Am. J. Phys.* **35** 177
[12] Goldberger M L and Watson K M 1964 *Collision Theory* (New York: Wiley) ch 6
[13] Nacher P J and Dupont-Roc J 1991 *Phys. Rev. Lett.* **67** 2966